Geophysical Research Letters

RESEARCH LETTER
10.1029/2024GL109925

Honeycomb-Like Magnetosheath Structure Formed by Jets: Three-Dimensional Global Hybrid Simulations

Junyi Ren[1], Jin Guo[1], Quanming Lu[1,2,3], San Lu[1,2,3], Xinliang Gao[1,2,3], Jiuqi Ma[1], and Rongsheng Wang[1,2,3]

[1]CAS Key Lab of Geospace Environment, School of Earth and Space Sciences, University of Science and Technology of China, Hefei, China, [2]Deep Space Exploration Laboratory, CAS Center for Excellent in Comparative Planetology, Hefei, China, [3]Collaborative Innovation Center of Astronautical Science and Technology, Harbin, China

Key Points:

- Magnetosheath jets are studied by a realistic-scale, 3-D global hybrid simulation under a radial interplanetary magnetic field (IMF)
- The magnetosheath has a honeycomb-like 3D structure where regions of increased dynamic pressure surround those of decreased dynamic pressure
- The magnetosheath jets formed at the quasi-parallel shock can propagate to the magnetosheath downstream of the quasi-perpendicular shock

Correspondence to:

J. Guo and Q. Lu,
gj0507@mail.ustc.edu.cn;
qmlu@ustc.edu.cn

Citation:

Ren, J., Guo, J., Lu, Q., Lu, S., Gao, X., Ma, J., & Wang, R. (2024). Honeycomb-like magnetosheath structure formed by jets: Three-dimensional global hybrid simulations. *Geophysical Research Letters*, *51*, e2024GL109925. https://doi.org/10.1029/2024GL109925

Received 22 APR 2024
Accepted 30 MAY 2024

Abstract Magnetosheath jets with enhanced dynamic pressure are common in the Earth's magnetosheath. They can impact the magnetopause, causing deformation of the magnetopause. Here we investigate the 3-D structure of magnetosheath jets using a realistic-scale, 3-D global hybrid simulation. The magnetosheath has an overall honeycomb-like 3-D structure, where the magnetosheath jets with increased dynamic pressure surround the regions of decreased dynamic pressure resembling honeycomb cells. The magnetosheath jets downstream of the bow shock region with $\theta_{Bn} \lesssim 20°$ (where θ_{Bn} is the angle between the upstream magnetic field and the shock normal) propagate approximately along the normal direction of the magnetopause, while those downstream of the bow shock region with $\theta_{Bn} \gtrsim 20°$ propagate almost tangential to the magnetopause. Therefore, some magnetosheath jets formed at the quasi-parallel shock region can propagate to the magnetosheath downstream of the quasi-perpendicular shock region.

Plain Language Summary Magnetosheath jets are high-speed transient structures frequently observed in the magnetosheath, and they can impact and dent the magnetopause. However, their three-dimensional (3-D) structure is still under debt despite decade-long research. By performing high-resolution, 3-D numerical simulation, we reveal that the magnetosheath has an overall honeycomb-like 3-D structure where the jets surround regions with lower plasma velocity resembling honeycomb cells.

1. Introduction

The interaction between the super-magnetosonic solar wind and the Earth's magnetic field forms the magnetosphere whose outer boundary is the magnetopause. The magnetosheath is located between the magnetopause and the bow shock that decelerates the solar wind from super-magnetosonic to sub-magnetosonic (Fairfield, 1971; Peredo et al., 1995). According to the angle (θ_{Bn}) between the shock normal direction and the interplanetary magnetic field (IMF), the bow shock is categorized into quasi-perpendicular ($\theta_{Bn} \gtrsim 45°$) and quasi-parallel ($\theta_{Bn} \lesssim 45°$). Solar wind particles reflected by the quasi-parallel shock can travel far upstream along the magnetic field lines, generating ion beam instabilities to excite ultra-low-frequency (ULF) waves (Hao et al., 2021; Lembege et al., 2004; Lu et al., 2020; Omidi, 2007; Quest, 1988; Su et al., 2012; Wu et al., 2015). These waves are carried to the magnetosheath by the solar wind and cause turbulence therein.

Magnetosheath jets, also known as high-speed jets, were first reported by Němeček et al. (1998) at Earth and are frequently observed in the magnetosheath downstream of the quasi-parallel shock (Archer et al., 2012; Plaschke et al., 2013). Within the magnetosheath jets, dynamic pressure increases and ion velocity often exceeds the local Alfvén speed, while the plasma temperature is lower and more isotropic than the surroundings (Archer & Horbury, 2013; Plaschke et al., 2013). It is well known that the magnetosheath jets can be formed by the interaction between the upstream waves and the quasi-parallel bow shock (Hietala et al., 2009; Palmroth et al., 2018; Raptis et al., 2022; Ren et al., 2023; Suni et al., 2021). The magnetosheath jets can drive bow waves inside the magnetosheath (Hietala et al., 2009; Liu et al., 2019; Ren et al., 2024), and impact the magnetopause to trigger localized magnetopause indentation (Shue et al., 2009; Yang et al., 2024), reconnection (Hietala et al., 2018), and magnetopause surface waves (Archer et al., 2019). The magnetosheath jets are more likely to reach the magnetopause when the IMF is quasi-radial (LaMoury et al., 2021). Guo et al. (2022) suggested that the alignment between the IMF and the solar wind velocity favors the formation of large magnetosheath jets. Further, Ren et al. (2023) found that the large magnetosheath jets form when upstream compressive structures continuously interact with the bow shock at specific regions. These large magnetosheath jets transport more mass and energy

from the solar wind and thus have a more significant influence on the Earth's magnetosphere (Plaschke et al., 2016).

To statistically analyze the scale sizes of magnetosheath jets, Plaschke et al. (2020) assumed the magnetosheath jets to be cylinder-like, whose axial directions are parallel to the propagation directions. They suggested that the magnetosheath jets have median scale sizes of 0.12 R_E and 0.15 R_E in the parallel and perpendicular directions, respectively. Using multi-spacecraft observations, Karlsson et al. (2012) found that the plasmoids, which are related structures to the magnetosheath jets, have pancake-like structures ("flattened flux tubes") with one dimension shorter than the others. Omelchenko et al. (2021) also demonstrated pancake-like jets using three-dimensional (3-D) global hybrid simulations, where the jets have three characteristic sizes: 4 R_E in the parallel direction, 6 R_E in the dawn-dusk direction, and 0.6 R_E in the north-south direction. However, their simulations reduce the scale of the Earth's magnetosphere, which may lead to unrealistic results.

In this study, we conducted a realistic-scale, 3-D global hybrid simulation to demonstrate that the magnetosheath has a honeycomb-like 3-D structure where jets with increased dynamic pressure surround magnetosheath cavities with decreased dynamic pressure (Guo et al., 2022; Katırcıoğlu et al., 2009; Omidi et al., 2016). Our results also indicate that the magnetosheath jets formed downstream of the quasi-parallel shock can propagate to the magnetosheath downstream of the quasi-perpendicular shock, which may be a source of jets downstream of the quasi-perpendicular shock.

2. Simulation Model

This study utilizes a three-dimensional global hybrid simulation model (Lin & Wang, 2005). In hybrid simulations, ions are treated as particles while electrons are treated as a massless, charge-neutralizing fluid. The displacement current is neglected, the electric field is solved through Ohm's law, and the magnetic field is advanced by Faraday's law. The simulation is performed in a spherical coordinate system (r, θ, φ), encompassing a simulation domain of the geocentric distance $3\ R_E \le r \le 30\ R_E$, polar angle $-10° \le \theta \le 190°$, and azimuth angle $20° \le \varphi \le 160°$. The simulation grid consists of $N_r \times N_\theta \times N_\varphi = 720 \times 420 \times 540$ cells. Within the inner magnetosphere ($r \le 6.5\ R_E$), a cold, incompressible ion fluid is filled to represent the plasmasphere.

Grid spacing in the r direction is nonuniform, with $\Delta r \simeq 0.02 R_E$ within $8\ R_E \le r \le 14\ R_E$ and being larger elsewhere. This setup keeps high resolution in the magnetosheath region while reducing the computational costs. Outflow (open) boundary conditions are applied to all boundaries for particles (fields), except for a conductive field boundary at the inner boundary ($r = 3\ R_E$) and the injection of solar wind particles at the outer boundary ($r = 30\ R_E$). The simulation results are presented in geocentric solar-magnetospheric (GSM) coordinates, with the x-axis points from the Earth's center to the Sun, the z-axis aligned with the Earth's dipole axis, and the y-axis completing the right-handed coordinates system. The simulation time step is $\Delta t = 0.02\ \Omega_i^{-1}$, where the ion gyrofrequency Ω_i^{-1} is determined by the solar wind magnetic field. The initial state involves about 8×10^9 macroparticles, and a small, current-dependent collision frequency is used to simulate anomalous resistivity and trigger magnetic reconnection. In the solar wind, the plasma number density is $N_i = 3.2\ \mathrm{cm}^{-3}$, and the magnetic field is $\mathbf{B} = (3.72, -0.13, 0.21)$ nT. The plasma beta values for ions and electrons are $\beta_i = \beta_e = 0.22$, and the solar wind velocity is $\mathbf{V}_{SW} = (-466.48, -12.86, -14.31)$ km/s. The Alfvén Mach number is therefore $M_A = 12.27$. In our simulation, for the first time, a realistic magnetosphere scale is used, where $1\ R_E = 50\ d_{i0}$, with d_{i0} representing the ion inertial length in the solar wind. Additionally, to study the effect of reducing magnetosphere scale on the 3-D structure of magnetosheath jets, another simulation is also performed with a reduced scale where $1\ R_E = 10\ d_{i0}$ (5 times smaller than reality), while other parameters are kept identical to those of the realistic-scale case described above. Because the Alfvén speed, which measures the evolution speed of kinetic effects, is larger relative to the magnetosphere scale size in the reduced-scale case, the magnetosphere evolves faster than in the realistic-scale case. For a direct comparison of the two cases, the simulation time in the reduced-scale case is presented 5 times larger.

3. Simulation Results

An overview of the realistic-scale case under a radial IMF is shown in Figure 1. The bow shock results from the interaction between the solar wind and the geomagnetic field, with the magnetosheath situated downstream of the bow shock. The bow shock is quasi-parallel and rippled around the subsolar region while being quasi-

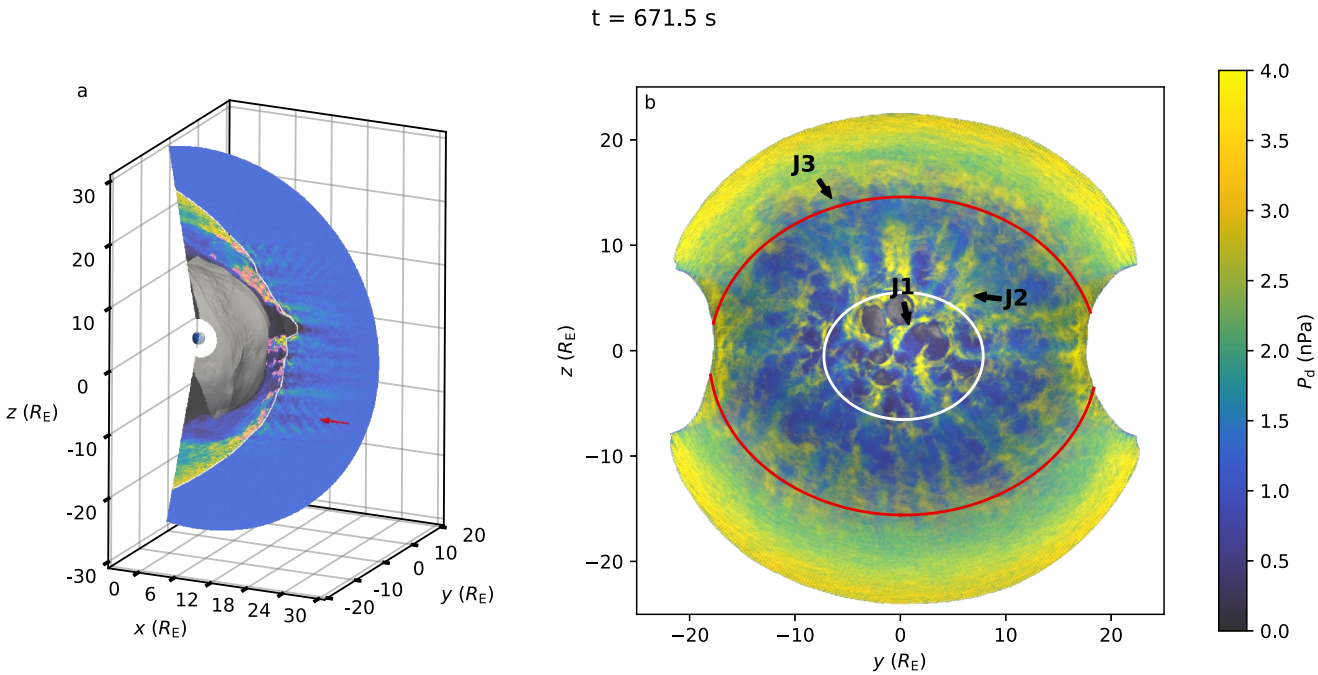

Figure 1. Overview of the honeycomb-like magnetosheath structure driven by jets at $t = 671.5$ s. (a) Dynamic pressure P_d in the noon-midnight meridian plane. The gray surface is the magnetopause identified by the boundary of open/closed magnetic field lines. The pink contour indicates where the dynamic pressure is two times the background value in the magnetosheath, as defined in Archer and Horbury (2013). (b) Dynamic pressure in the magnetosheath. The white and red curves indicate the bow shock with $\theta_{Bn} = 20°$ and 45°, respectively.

perpendicular around the flank region. Downstream of both quasi-parallel and quasi-perpendicular bow shock, many magnetosheath jets with high dynamic pressure are observed, and some of them impact and dent the magnetopause. In Figure 1b, elliptical magnetosheath cavities with low dynamic pressure are surrounded by magnetosheath jets, illustrating an overall honeycomb-like 3-D structure in the magnetosheath, where the cavities and jets resemble honeycomb cells and their edges. Once the jets form downstream of the quasi-parallel shock, they propagate toward the flank region along the magnetosheath plasma flow.

The magnetosheath jets downstream of the bow shock with $\theta_{Bn} < 20°$ are shown in Figure 2. Figures 2b–2e plot the dynamic pressure and ion temperature of one magnetosheath jet ("J1") at $t = 671.5$ s in two perpendicular slices (pink and cyan slices in Figure 2a). Inside "J1," the ion temperature is decreased and is more isotropic than the surroundings, because the plasma from the solar wind is less heated by the bow shock in the magnetosheath jets. The parallel scale size of "J1" is about 3 R_E, and its perpendicular scale sizes are about 3 R_E and 0.4 R_E in the pink and cyan slices, respectively. This indicates a pancake-like localized structure for "J1," formed by being the edge of two magnetosheath cavities (Figure 1b). Additionally, some magnetosheath jets are located at the vertices of multiple magnetosheath cavities, whose localized 3-D structures are approximately cylinder-like (Figure 1b). "J1" impacts the magnetopause along the normal direction of the magnetopause, causing a localized magnetopause indentation. The magnetopause is dented more severely as "J1" continuously compresses the magnetopause in later times and expands back beyond its original location (not shown), as suggested by Němeček et al. (2023). Moreover, "J1" is meandering in the cyan slice (Figures 2c and 2e), which may be caused by Kelvin–Helmholtz instability (Guo et al., 2022).

Figure 3 shows magnetosheath jets downstream of the bow shock with $20° < \theta_{Bn} < 45°$. The magnetosheath jet "J2" forms at the bow shock where θ_{Bn} is about 20°, and propagates toward the flank region along the background plasma flow. Similar to "J1," the ion temperature inside "J2" also decreases (Figures 3d and 3e). The parallel scale size of "J2" is about 9 R_E and its perpendicular scale sizes are about 2.8 R_E and 1 R_E, indicating a ribbon-like localized 3-D structure. Within the honeycomb-like magnetosheath structure, the jets in the realistic-scale simulation can have different localized structures than just a cylinder or pancake shape suggested by previous studies (Omelchenko et al., 2021; Plaschke et al., 2016, 2018). "J2" propagates almost tangential to the magnetopause, and there is almost no inward pressure to the magnetopause in "J2" (Figure 3f). Therefore, no

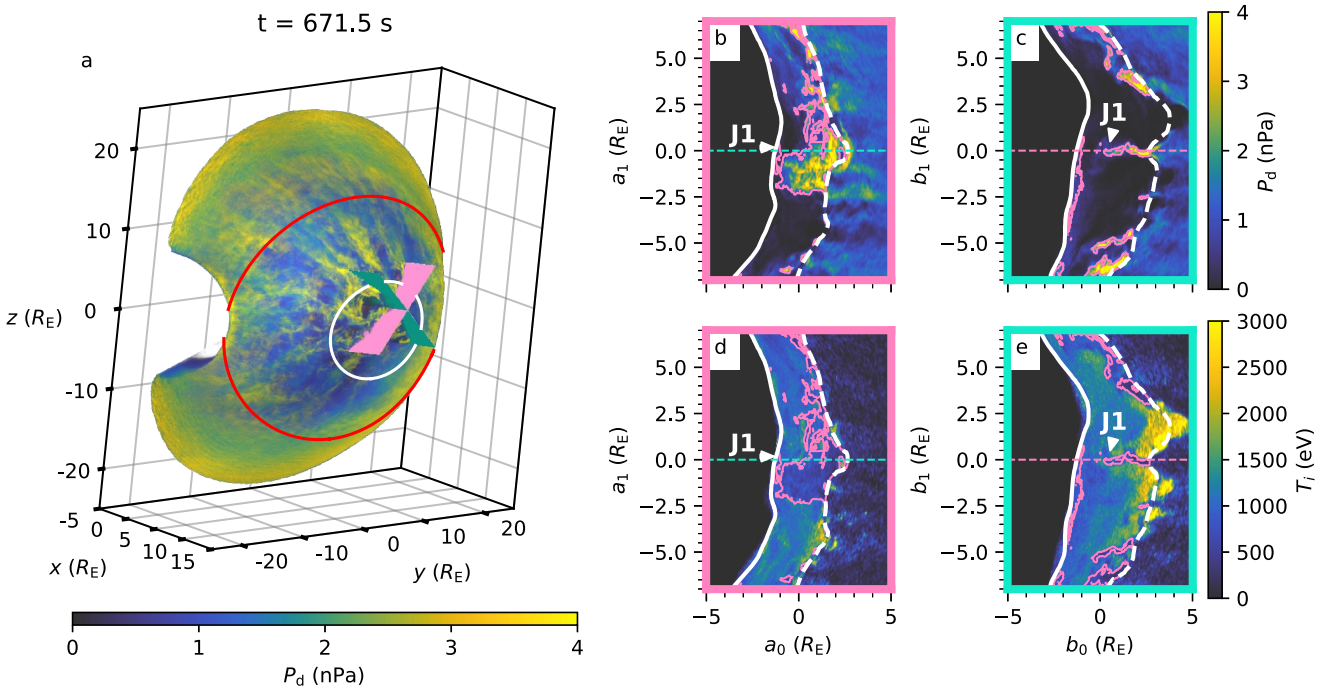

Figure 2. Magnetosheath jets downstream of the bow shock with $\theta_{Bn} < 20°$ at $t = 671.5$ s (a) 3-D view of the dynamic pressure P_d of the jets. The white and red curves indicate the bow shock with $\theta_{Bn} = 20°$ and 45°, respectively. The original point of both the pink and cyan slices is (12.8, 0.77, 2.07) R_E, while their normal directions are (−0.07, −0.697, 0.713) and (0.153, −0.715, −0.683), respectively. (b–c) Dynamic pressure P_d in the pink slice (b) and cyan slice (c). (d–e) Ion temperature T_i in the pink (d) and cyan (e) slices. The solid white curves indicate the magnetopause, and the dashed white curves indicate the bow shock.

obvious magnetopause indentation is caused. Magnetosheath jets like "J2" that form downstream of the bow shock with larger θ_{Bn} (>20° in our simulation) may have minor effects on the magnetopause.

Some magnetosheath jets can propagate long distances, even enter the magnetosheath downstream of the quasi-perpendicular bow shock. Figure 4 shows some magnetosheath jets downstream of the bow shock with $\theta_{Bn} > 45°$. Magnetosheath jets "J3"–"J5" are identified by dynamic pressure exceeding 1.5 times the magnetosheath background value. "J3"–"J5" also have ribbon-like localized structures and decreased temperature (Figures 4f–4i), but are weaker than those downstream of the quasi-parallel bow shock. At $t = 559.6$ s (Figures 4b and 4f), "J3" is located in the magnetosheath downstream of the quasi-parallel bow shock. "J3" then propagates along the magnetosheath plasma flow (Figures 4c and 4d) and enters the downstream magnetosheath of the quasi-perpendicular bow shock. At $t = 559.6$ s (Figure 4b), magnetosheath jets "J4" and "J5" are formed at the bow shock where θ_{Bn} is about 45°. "J4" and "J5" also propagate long distances (about 10 R_E and 5 R_E, respectively) in the magnetosheath and have entered the magnetosheath downstream of quasi-perpendicular bow shock at $t = 671.5$ s.

4. Discussion

Although magnetosheath jets have been studied for over a decade, their 3-D structure has always been under debate (Karlsson et al., 2012; Omelchenko et al., 2021; Plaschke et al., 2016). By performing a 3-D global hybrid simulation with realistic scale, we find that magnetosheath jets and cavities form an overall honeycomb-like 3-D magnetosheath structure, while the localized 3-D structure of the jets can be pancake-like, cylinder-like, ribbon-like, etc. To demonstrate the significance of the realistic scaling, a reduced-scale simulation with 1 $R_E = 10\ d_{i0}$ is also performed for comparison. Figure 5 shows the magnetosheath jets in the reduced-scale case at $t = 840.2$ s. There are only 3 jets-surrounded magnetosheath cavities in this case (Figure 5a), while there are about 16 in the realistic-scale case (Figure 1b). The maximum diameters of the magnetosheath cavities are about 8 R_E and 3 R_E in this reduced-scale case and the realistic-scale one, respectively. Moreover, in Figures 5b–5e, the parallel size of "J1′" is about 4 R_E, with perpendicular sizes of about 5.2 R_E and 0.8 R_E. Therefore, in the reduced-scale case, like

10.1029/2024GL109925

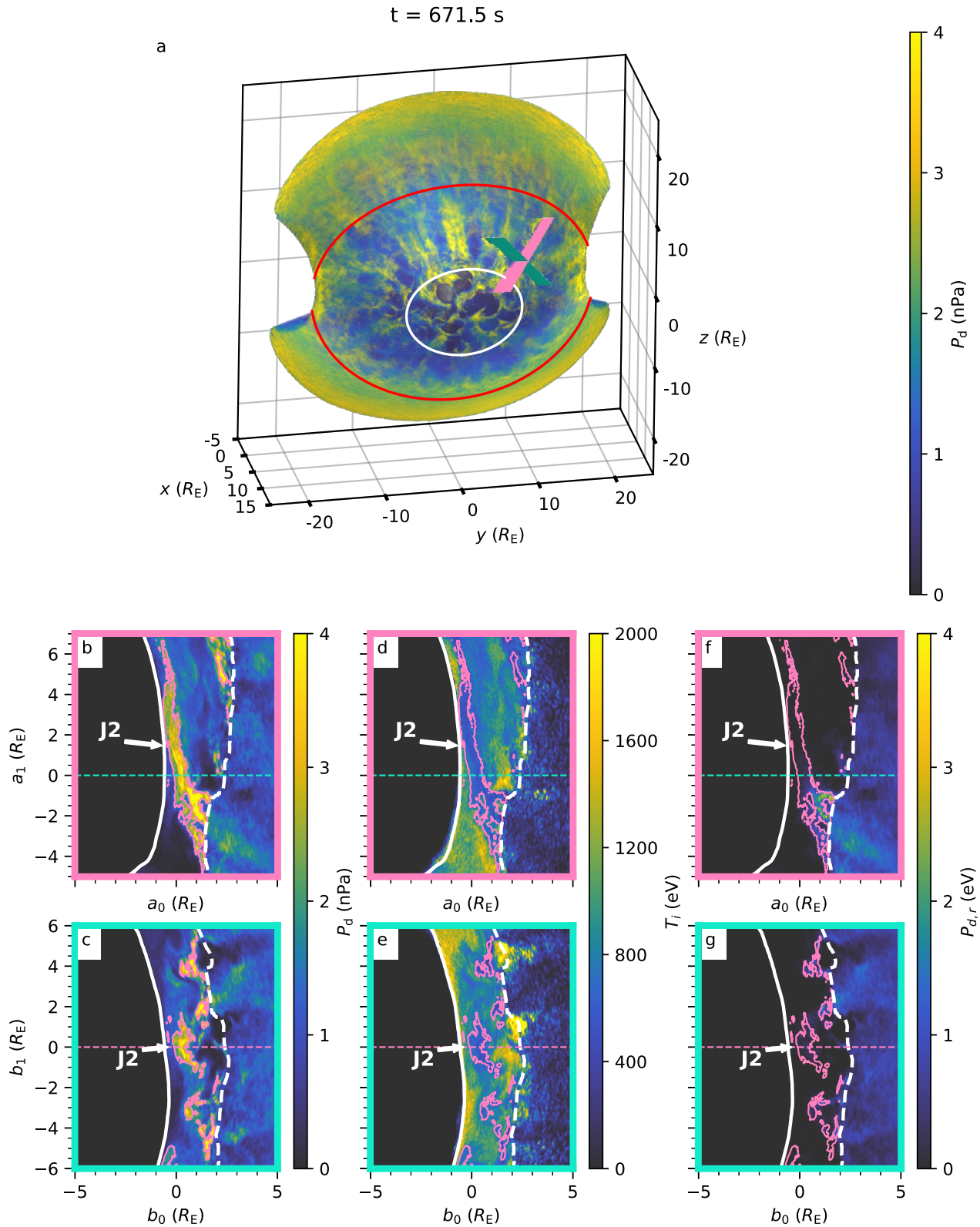

Figure 3. Magnetosheath jets downstream of the bow shock with $20° < \theta_{Bn} < 45°$ at $t = 671.5$ s (a) 3-D view of the jets. The original point of both the pink and cyan slices is (10.6, 6.05, 4.56) R_E, while their normal directions are (0.050, −0.656, 0.753) and (0.580, −0.594, −0.557), respectively. (b–c) Dynamic pressure P_d, (d–e) ion temperature T_i, (f–g) r component of the dynamic pressure $P_{d,r}$. The variables are taken from the pink (b, d, f) and cyan (c, e, g) slices. The solid white curves indicate the magnetopause, and the dashed white curves indicate the bow shock.

10.1029/2024GL109925

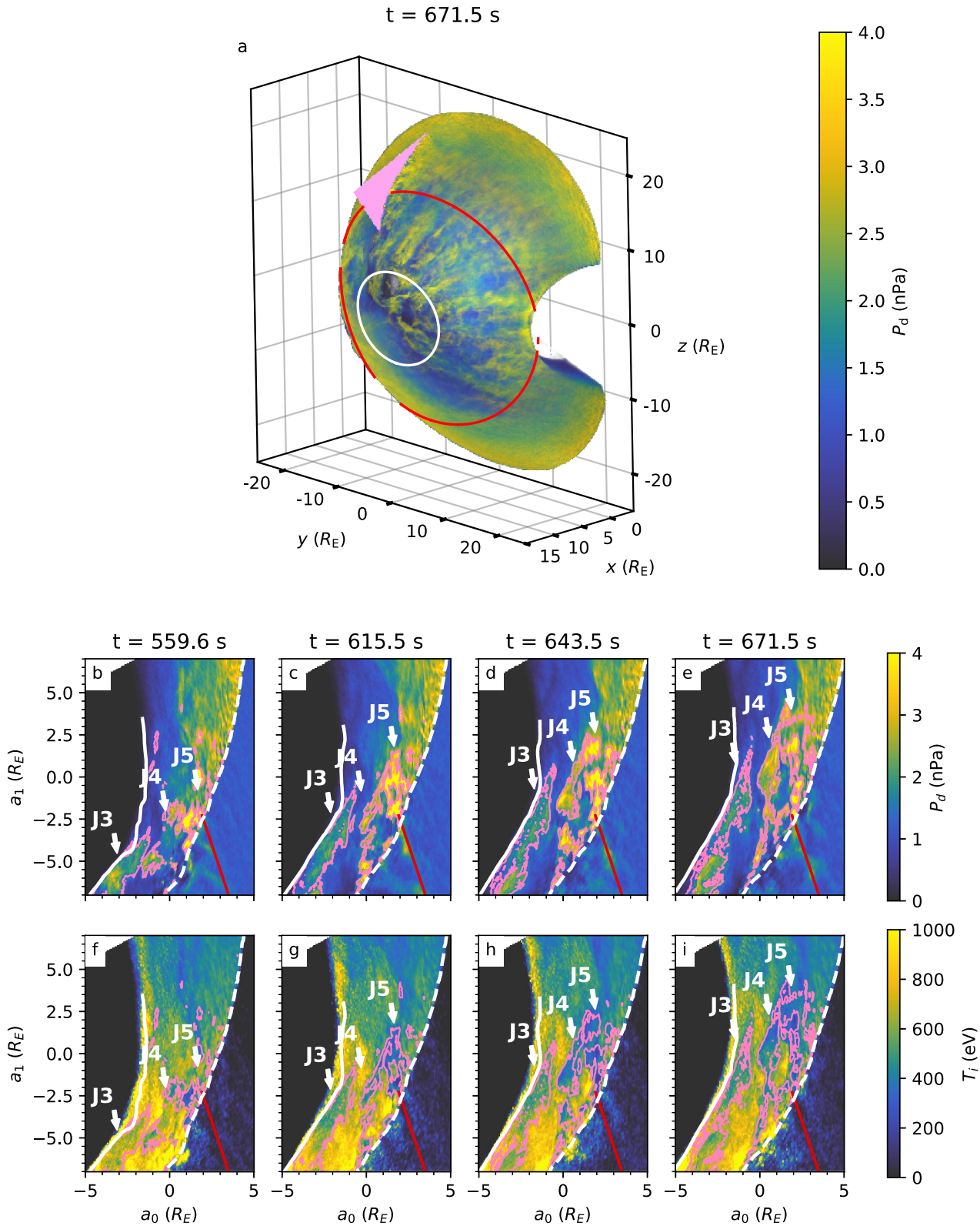

Figure 4. Magnetosheath jets downstream of the bow shock with $\theta_{Bn} > 45°$. (a) 3-D view of the jets at $t = 671.5$ s. The original point of the pink slice is (4.85, −6.09, 12.6) R_E, and its normal direction is (−0.143, −0.911, −0.386). (b–e) Dynamic pressure P_d in the pink slice $t = 559.6$ s, 615.5 s, 643.5 s, and 671.5 s (f–i) Ion temperature T_i in the pink slice at the same times. The solid white curves indicate the magnetopause, and the dashed white curves indicate the bow shock.

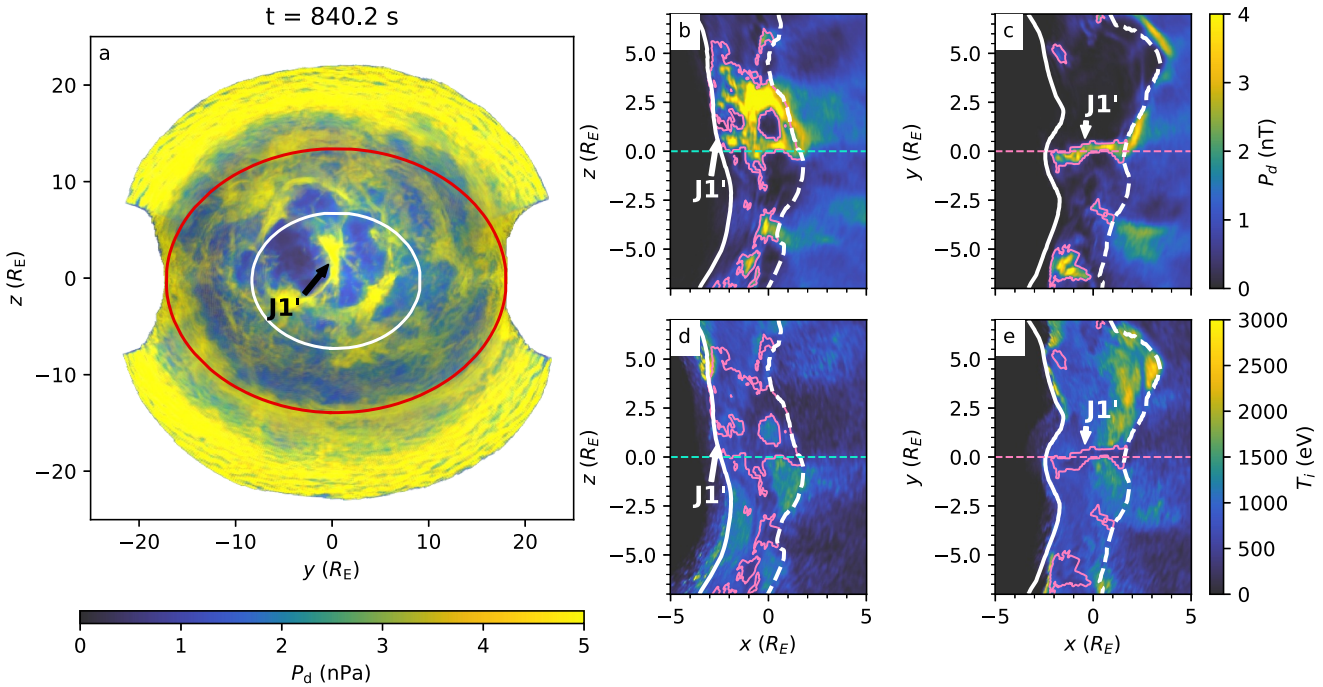

Figure 5. Magnetosheath jets at $t = 840.2$ s obtained from the reduced-scale case where 1 $R_E = 10\ d_{i0}$. (a) Dynamic pressure P_d in the magnetosheath. The white and red curves indicate the bow shock with $\theta_{Bn} = 20°$ and 45°, respectively. (b–c) Dynamic pressure in the equatorial plane (b) and noon-midnight meridian plane (e). The solid white curves indicate the magnetopause, and the dashed white curves indicate the bow shock.

the ones performed by Omelchenko et al. (2021), the numbers of magnetosheath jets and cavities are underestimated, while their scale sizes are overestimated.

The small and numerous jets in the realistic-scale case can increase turbulence in the magnetosheath and lead to more magnetopause indentations. Moreover, jets with ribbon-like localized structures downstream of the bow shock with $\theta_{Bn} \gtrsim 20°$ are difficult to identify in the reduced-scale case. Only in the realistic-scale case do we find jets formed downstream of the quasi-parallel shock propagate downstream of the quasi-perpendicular shock. Therefore, global simulations with a reduced-scale magnetosphere may not effectively capture physical processes related to the bow shock. The scale sizes of many foreshock structures, such as spontaneous hot flow anomalies (Omidi et al., 2013; Zhang et al., 2013), magnetosheath cavities (Guo et al., 2022; Katırcıoğlu et al., 2009; Omidi et al., 2016), and foreshock bubbles (C. Wang et al., 2021; B. Wang et al., 2020), may be related to the scale size of the magnetosphere. Using a 3-D global hybrid simulation with a reduced-scale magnetosphere (1 $R_E = 12\ d_{i0}$), Ng et al. (2023) showed that kinetic structures like foreshock cavitons can be seen through soft X-ray imaging. However, it is possible that the scale size of the foreshock cavitons was overestimated in their simulation results.

5. Conclusions

In this study, we investigate the 3-D structure of magnetosheath jets using a realistic-scale, 3-D global hybrid simulation. The magnetosheath has an overall honeycomb-like 3-D structure, where the magnetosheath jets surround magnetosheath cavities like honeycomb cells. The magnetosheath jets downstream of the bow shock with $\theta_{Bn} \lesssim 20°$ propagate approximately along the normal direction of the magnetopause, while those downstream of the bow shock with $\theta_{Bn} \gtrsim 20°$ propagate almost tangential to the magnetopause. Moreover, some magnetosheath jets formed downstream of quasi-parallel shock can propagate to the magnetosheath downstream of the quasi-perpendicular shock and become a source of jets therein, which is shown in the realistic-scale simulation but not in the reduced-scale one. Our results highlight the necessity of realistic-scale simulation models to study the structures related to the bow shock.

Data Availability Statement

The simulation data (Ren & Guo, 2024) used to plot the figures in this paper can be downloaded from "National Space Science Data Center, National Science and Technology Infrastructure of China".

Acknowledgments
This work was supported by NSFC Grant numbers 42230201, 4217481 and the Strategic Priority Research Program of Chinese Academy of Sciences Grant number XDB41000000. Computer resources were provided by the Hefei Advanced Computing Center of China, and the data hosting service is provided by the "National Space Science Data Center, National Science and Technology Infrastructure of China (www.nssdc.ac.cn)".

References

Archer, M. O., Hietala, H., Hartinger, M. D., Plaschke, F., & Angelopoulos, V. (2019). Direct observations of a surface Eigen mode of the dayside magnetopause. *Nature Communications*, *10*(1), 615. https://doi.org/10.1038/s41467-018-08134-5

Archer, M. O., & Horbury, T. S. (2013). Magnetosheath dynamic pressure enhancements: Occurrence and typical properties. *Annales Geophysicae*, *31*(2), 319–331. https://doi.org/10.5194/angeo-31-319-2013

Archer, M. O., Horbury, T. S., & Eastwood, J. P. (2012). Magnetosheath pressure pulses: Generation downstream of the bow shock from solar wind discontinuities. *Journal of Geophysical Research*, *117*(A5). https://doi.org/10.1029/2011ja017468

Fairfield, D. H. (1971). Average and unusual locations of the earth's magnetopause and bow shock. *Journal of Geophysical Research*, *76*(28), 6700–6716. https://doi.org/10.1029/ja076i028p06700

Guo, J., Lu, S., Lu, Q., Lin, Y., Wang, X., Ren, J., et al. (2022). Large-scale high-speed jets in earth's magnetosheath: Global hybrid simulations. *Journal of Geophysical Research: Space Physics*, *127*(6). https://doi.org/10.1029/2022ja030477

Hao, Y., Lu, Q., Wu, D., Lu, S., Xiang, L., & Ke, Y. (2021). Low-frequency waves upstream of quasi-parallel shocks: Two-dimensional hybrid simulations. *The Astrophysical Journal*, *915*(1), 64. https://doi.org/10.3847/1538-4357/ac02ce

Hietala, H., Laitinen, T. V., Andréeová, K., Vainio, R., Vaivads, A., Palmroth, M., et al. (2009). Supermagnetosonic jets behind a collisionless quasiparallel shock. *Physical Review Letters*, *103*(24), 245001. https://doi.org/10.1103/physrevlett.103.245001

Hietala, H., Phan, T. D., Angelopoulos, V., Oieroset, M., Archer, M. O., Karlsson, T., & Plaschke, F. (2018). In situ observations of a magnetosheath high-speed jet triggering magnetopause reconnection. *Geophysical Research Letters*, *45*(4), 1732–1740. https://doi.org/10.1002/2017gl076525

Karlsson, T., Brenning, N., Nilsson, H., Trotignon, J., Vallières, X., & Facsko, G. (2012). Localized density enhancements in the magnetosheath: Three-dimensional morphology and possible importance for impulsive penetration. *Journal of Geophysical Research*, *117*(A3). https://doi.org/10.1029/2011ja017059

Katırcıoğlu, F. T., Kaymaz, Z., Sibeck, D. G., & Dandouras, I. (2009). Magnetosheath cavities: Case studies using cluster observations. *Annales Geophysicae*, *27*(10), 3765–3780. https://doi.org/10.5194/angeo-27-3765-2009

LaMoury, A. T., Hietala, H., Plaschke, F., Vuorinen, L., & Eastwood, J. P. (2021). Solar wind control of magnetosheath jet formation and propagation to the magnetopause. *Journal of Geophysical Research: Space Physics*, *126*(9). https://doi.org/10.1029/2021ja029592

Lembege, B., Giacalone, J., Scholer, M., Hada, T., Hoshino, M., Krasnoselskikh, V., et al. (2004). Selected problems in collisionless-shock physics. *Space Science Reviews*, *110*(3/4), 161–226. https://doi.org/10.1023/b:spac.0000023372.12232.b7

Lin, Y., & Wang, X. Y. (2005). Three-dimensional global hybrid simulation of dayside dynamics associated with the quasi-parallel bow shock. *Journal of Geophysical Research*, *110*(A12). https://doi.org/10.1029/2005ja011243

Liu, T. Z., Hietala, H., Angelopoulos, V., Omelchenko, Y., Roytershteyn, V., & Vainio, R. (2019). THEMIS observations of particle acceleration by a magnetosheath jet-driven bow wave. *Geophysical Research Letters*, *46*(14), 7929–7936. https://doi.org/10.1029/2019gl082614

Lu, Q., Wang, H., Wang, X., Lu, S., Wang, R., Gao, X., & Wang, S. (2020). Turbulence-driven magnetic reconnection in the magnetosheath downstream of a quasi-parallel shock: A three-dimensional global hybrid simulation. *Geophysical Research Letters*, *47*(1). https://doi.org/10.1029/2019gl085661

Němeček, Z., Šafránková, J., Grygorov, K., Mokrý, A., Pi, G., Aghabozorgi Nafchi, M., et al. (2023). Extremely distant magnetopause locations caused by magnetosheath jets. *Geophysical Research Letters*, *50*(24). https://doi.org/10.1029/2023gl106131

Němeček, Z., Šafránková, J., Přech, L., Sibeck, D. G., Kokubun, S., & Mukai, T. (1998). Transient flux enhancements in the magnetosheath. *Geophysical Research Letters*, *25*(8), 1273–1276. https://doi.org/10.1029/98gl50873

Ng, J., Walsh, B. M., Chen, L., & Omelchenko, Y. (2023). Soft X-ray imaging of earth's dayside magnetosheath and cusps using hybrid simulations. *Geophysical Research Letters*, *50*(10). https://doi.org/10.1029/2023gl103347

Omelchenko, Y. A., Chen, L.-J., & Ng, J. (2021). 3D space-time adaptive hybrid simulations of magnetosheath high-speed jets. *Journal of Geophysical Research: Space Physics*, *126*(7). https://doi.org/10.1029/2020ja029035

Omidi, N. (2007). Formation of cavities in the foreshock. In *AIP conference proceedings* (Vol. 932, pp. 181–190). American Institute of Physics. https://doi.org/10.1063/1.2778962

Omidi, N., Berchem, J., Sibeck, D., & Zhang, H. (2016). Impacts of spontaneous hot flow anomalies on the magnetosheath and magnetopause. *Journal of Geophysical Research: Space Physics*, *121*(4), 3155–3169. https://doi.org/10.1002/2015ja022170

Omidi, N., Zhang, H., Sibeck, D., & Turner, D. (2013). Spontaneous hot flow anomalies at quasi-parallel shocks: 2. Hybrid simulations. *Journal of Geophysical Research: Space Physics*, *118*(1), 173–180. https://doi.org/10.1029/2012ja018099

Palmroth, M., Hietala, H., Plaschke, F., Archer, M., Karlsson, T., Blanco-Cano, X., et al. (2018). Magnetosheath jet properties and evolution as determined by a global hybrid-VLASOV simulation. *Annales Geophysicae*, *36*(5), 1171–1182. https://doi.org/10.5194/angeo-36-1171-2018

Peredo, M., Slavin, J. A., Mazur, E., & Curtis, S. A. (1995). Three-dimensional position and shape of the bow shock and their variation with Alfvénic, sonic and magnetosonic mach numbers and interplanetary magnetic field orientation. *Journal of Geophysical Research*, *100*(A5), 7907–7916. https://doi.org/10.1029/94ja02545

Plaschke, F., Hietala, H., & Angelopoulos, V. (2013). Anti-sunward high-speed jets in the subsolar magnetosheath. *Annales Geophysicae*, *31*(10), 1877–1889. https://doi.org/10.5194/angeo-31-1877-2013

Plaschke, F., Hietala, H., Angelopoulos, V., & Nakamura, R. (2016). Geoeffective jets impacting the magnetopause are very common. *Journal of Geophysical Research: Space Physics*, *121*(4), 3240–3253. https://doi.org/10.1002/2016ja022534

Plaschke, F., Hietala, H., Archer, M., Blanco-Cano, X., Kajdič, P., Karlsson, T., et al. (2018). Jets downstream of collisionless shocks. *Space Science Reviews*, *214*(5), 81. https://doi.org/10.1007/s11214-018-0516-3

Plaschke, F., Hietala, H., & Vörös, Z. (2020). Scale sizes of magnetosheath jets. *Journal of Geophysical Research: Space Physics*, *125*(9). https://doi.org/10.1029/2020ja027962

Quest, K. B. (1988). Theory and simulation of collisionless parallel shocks. *Journal of Geophysical Research*, *93*(A9), 9649–9680. https://doi.org/10.1029/ja093ia09p09649

Raptis, S., Karlsson, T., Vaivads, A., Pollock, C., Plaschke, F., Johlander, A., et al. (2022). Downstream high-speed plasma jet generation as a direct consequence of shock reformation. *Nature Communications*, *13*(1), 598. https://doi.org/10.1038/s41467-022-28110-4

Ren, J., & Guo, J. (2024). Data for "the formation of honeycomb-like magnetosheath jets: Three-dimensional global hybrid simulations" [Dataset]. *Science Data Bank*. https://doi.org/10.57760/sciencedb.18059

Ren, J., Lu, Q., Gao, X., Gedalin, M., Qiu, H., Han, D., & Wang, R. (2024). Hybrid simulation of magnetosheath jet-driven bow waves. *Geophysical Research Letters*, *51*(5). https://doi.org/10.1029/2023gl106606

Ren, J., Lu, Q., Guo, J., Gao, X., Lu, S., Wang, S., & Wang, R. (2023). Two-dimensional hybrid simulations of high-speed jets downstream of quasi-parallel shocks. *Journal of Geophysical Research: Space Physics*, *128*(8). https://doi.org/10.1029/2023ja031699

Shue, J., Chao, J., Song, P., McFadden, J. P., Suvorova, A., Angelopoulos, V., et al. (2009). Anomalous magnetosheath flows and distorted subsolar magnetopause for radial interplanetary magnetic fields. *Geophysical Research Letters*, *36*(18). https://doi.org/10.1029/2009gl039842

Su, Y., Lu, Q., Huang, C., Wu, M., Gao, X., & Wang, S. (2012). Particle acceleration and generation of diffuse superthermal ions at a quasi-parallel collisionless shock: Hybrid simulations. *Journal of Geophysical Research*, *117*(A8). https://doi.org/10.1029/2012ja017736

Suni, J., Palmroth, M., Turc, L., Battarbee, M., Johlander, A., Tarvus, V., et al. (2021). Connection between foreshock structures and the generation of magnetosheath jets: Vlasiator results. *Geophysical Research Letters*, *48*(20). https://doi.org/10.1029/2021gl095655

Wang, B., Liu, T., Nishimura, Y., Zhang, H., Hartinger, M., Shi, X., et al. (2020). Global propagation of magnetospheric PC5 ULF waves driven by foreshock transients. *Journal of Geophysical Research: Space Physics*, *125*(12). https://doi.org/10.1029/2020ja028411

Wang, C., Wang, X., Liu, T. Z., & Lin, Y. (2021). A foreshock bubble driven by an IMF tangential discontinuity: 3D global hybrid simulation. *Geophysical Research Letters*, *48*(9). https://doi.org/10.1029/2021gl093068

Wu, M., Hao, Y., Lu, Q., Huang, C., Guo, F., & Wang, S. (2015). The role of large amplitude upstream low-frequency waves in the generation of superthermal ions at a quasi-parallel collisionless shock: *Cluster* observations. *The Astrophysical Journal*, *808*(1), 2. https://doi.org/10.1088/0004-637x/808/1/2

Yang, Z., Jarvinen, R., Guo, X., Sun, T., Koutroumpa, D., K. Parks, G., et al. (2024). Deformations at Earth's dayside magnetopause during quasi-radial IMF conditions: Global kinetic simulations and soft X-ray imaging. *Earth and Planetary Physics*, *8*(1), 59–69. https://doi.org/10.26464/epp2023059

Zhang, H., Sibeck, D. G., Zong, Q.-G., Omidi, N., Turner, D., & Clausen, L. B. N. (2013). Spontaneous hot flow anomalies at quasi-parallel shocks: 1. Observations. *Journal of Geophysical Research: Space Physics*, *118*(6), 3357–3363. https://doi.org/10.1002/jgra.50376